waterbouwkundig LABORATORIUM

Rijkswaterstaat
Ministerie van Infrastructuur en Milieu

Large Scale Embankment Breach Experiments in Flume

Gensheng Zhao, Paul Visser, Patrik Peeters

Version: 15042014

TU Delft Delft University of Technology

Challenge the future

Table of Contents

1 Introduction

Embankments, including Dikes and dams, are of large benefit to people all over the world. Since the beginning of human civilization thousands of years ago, embankments have been playing vital role in the development of human being. History of embankments is an epitome of the rise and fall of human civilization, especially on the defenses of floods and irrigations from rivers and lakes. Embankments, blocking the floods in the river channels, sea and lakes, have already been protecting human lives and properties from flood disasters; Embankment, impounding large volumes of waters, have already been used to flood control, navigation, irrigation, water supply, hydro-electric power, recreation and so on. However, embankments could also give human lives and properties high risks to some extend for their failures due to overtopping, piping and other factors. Further, embankments generated automatically by the nature are also providing risks, due to the landslides induced by the earthquakes, storms and so on.

The magnitude and extent of the losses depend highly on the rate of the breaching of embanks, which determines the discharge through the breach and the speed and rate of inundation of the polder, the areas outside the embankments or downstream. Therefore, modeling of breach evolution in embankments, predicting the breach parameters (e.g. depth, width, discharge) and the breach flow rate, is of significant interest for damage assessment and risk analysis. It is also important for the development of early warning system for dike and dam failures and evacuation plans of people at risk.

Ralston (1987) gave a good description of the mechanics of embankment erosion. For cohesive embankments, breaching takes place due to headcut erosion. At the beginning, the headcut is typically formed at the toe of the embankment and then advances upstream until the crest of the embankment is reached. In some cases a series of stair-step headcut forms on the downstream face of the embankment. The action is similar to that described by Dodge (1988) for model testing of embankment overtopping. The relevant processes are headcut initiation and advance by hydrodynamic and geotechnical mass wasting.

Zhu et al. (2004) summarized ongoing research efforts of several entities aimed at developing new methods for protecting embankments from erosion during overtopping flow, and for predicting erosion of protected and unprotected embankments. All of the studies indicate that embankment erosion is a multivariable, multidisciplinary problem. Random influences can be

substantial, and thus, repetition of model tests is essential. Fread (1988) developed a breach erosion model (BREACH) for an earthen dam to predict the breach size, shape, and time of formation and breach outflow hydrograph. In the model, erosion is assumed to occur equally along the bottom and sides of the breach channel except when the sides of the breach channel collapse and if the valley floor has been reached, further downwards erosion is not allowed and the peak discharge would be expected.

In the model of Visser (1998) for sand-dikes, a relatively small initial breach is assumed in the top of the dike that is so large that water flows through it starting the breach erosion process. By assuming a trapezoidal shape of the initial breach with the angle of repose, five stages can be distinguished in the process of breach erosion (Fig. 1):

1) Steepening of inner slope from the initial value up to a critical value.
2) Retrograde erosion of the inner slope of the dike in the breach, yielding a decrease of the width of the crest of the dike in the breach.
3) Lowering of the top of the dike in the breach, with constant angle of the critical breach side slopes, resulting in an increase of width of the breach.
4) Critical flow stage, in which the flow is virtually critical throughout the breach, and the breach continues to grow mainly laterally.
5) Subcritical flow stage, in which the breach continues to grow, mainly laterally.

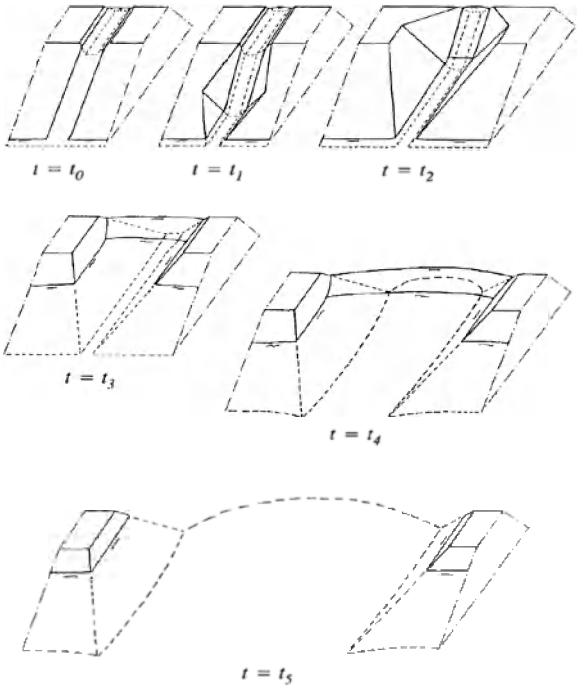

Figure 1 Schematic illustration of breach growth in a sand-dike (Visser, 1998)

In the first three stages the initial breach cuts itself into the dike; most of the discharge through the breach happens in stages 4 and 5.

Corresponding to the study of sand-dike breaching by Visser, Zhu (2006) investigated the breaching process of clay-dikes. The distinct difference from sand-dike breaching is the headcut erosion that occurs during the breaching process of clay-dikes. Similarly, by assuming an initial breach in the top of the dike that is relatively small and trapezoidal-shaped, Zhu (2006) classified the breach erosion process in clay-dikes into the five following stages:

1) Stage I ($t_0 < t < t_1$): Floodwater flows through the initial breach in the dike crest and erodes soil away from the crest and the inner slope of the dike. Both flow shear erosion as well as small-scale headcut erosion can occur along the inner slope (see Fig. 2(a)(b)).

2) Stage II ($t_1 < t < t_2$): The steepened inner slope of the dike holds the critical slope angle throughout Stage II and acts like a headcut during the erosion process owing to its large steepness (see Fig. 2(b)(c)).

3) Stage III ($t_2 < t < t_3$): The headcut still maintains the critical slope angle . The breach enlarges rapidly, accordingly also the flow rate through the breach, which in turn accelerates the breach erosion process in the dike. At the end of this stage, the dike body in the breach has been washed away completely down to the dike foundation or to the toe protection on the dike outer slope (see Fig. 2(c)(d)).

4) Stage IV ($t_3 < t < t_4$): In this stage the flow in the breach is critical. Breach erosion takes place mainly laterally, with flow shear erosion along the side-slopes of the breach and the resulting discrete side slope instability being the main mechanisms for the breach enlargement. Vertical erosion in this stage relies mainly on the geometrical and material features of the dike (see Fig. 2(d)(e)).

5) Stage V ($t_4 < t < t_5$): In this stage the breach flow is subcritical. The breach erosion still occurs mainly laterally and at the end, the velocity of the breach flow is reduced to such an extent that it can no longer erode away soil material from either the dike body or the dike foundation, hence the breach growth process stops (see Fig. 2(e)(f)).

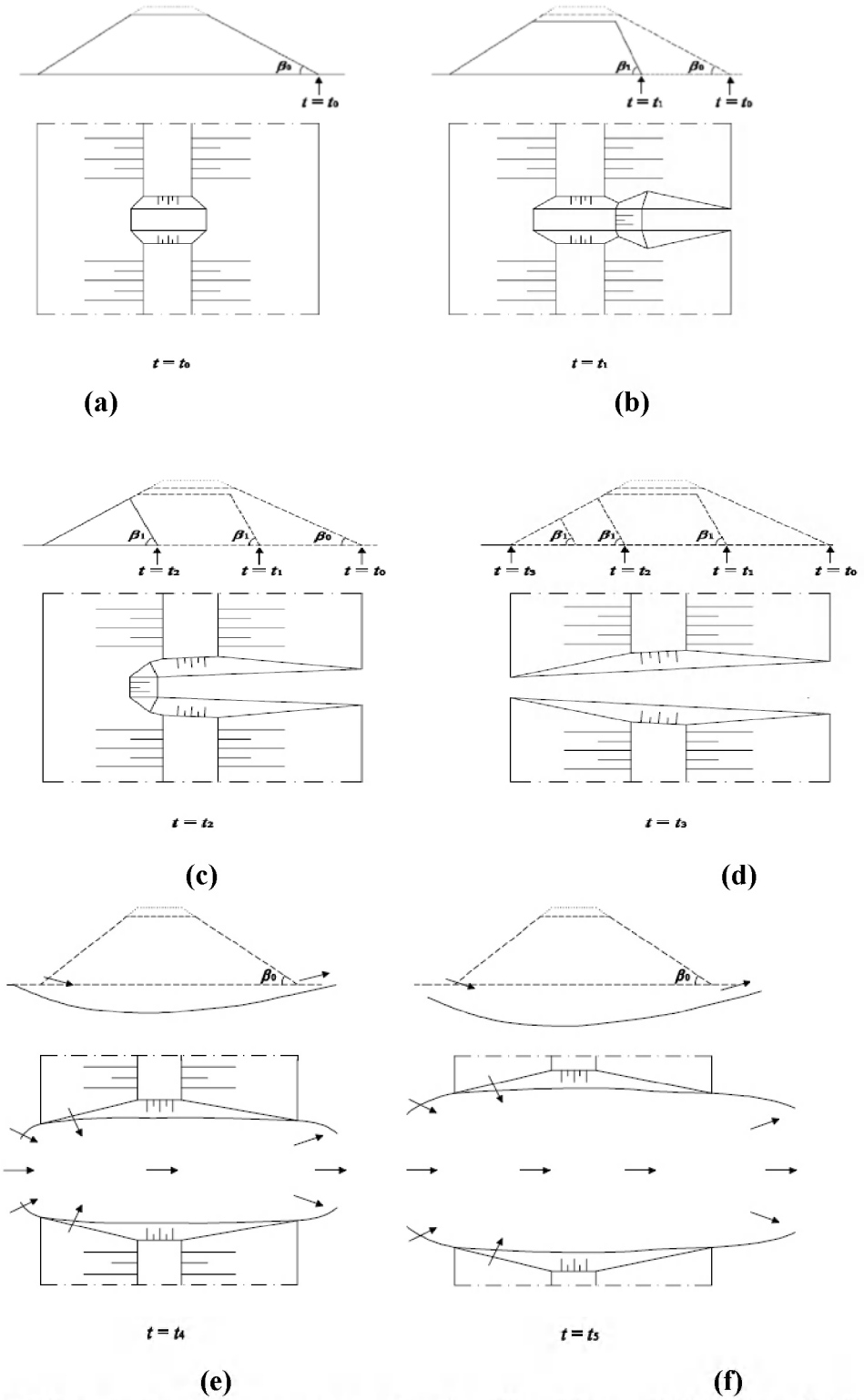

Figure 2 Breach development process in clay dike (Visser, 1998; Zhu, 2006)

Overtopping breaching is the most frequent form of embankment failure. The magnitude and extent of the losses depend highly on the rate of the breaching of embankments, which in turn determines the discharge through the breach and the speed and rate of inundation of the polder, the areas outside the embankments or downstream of the breach. Therefore, the

modeling of breach evolution in embankments, the predicting of the breach parameters (e.g. depth, width, discharge) and the breach flow rate, is of significant interest to damage assessment and risk analysis. It is also important for the development of early warning systems for dike and dam failures and for evacuation plans of people at risk.

The embankment breaching process can be divided into several stages according to the researcher's hypothesis and the prototype surveys, lab experiments. Researchers have different methods to classify the breaching processes because of the embankment different materials. In order to reveal the physical process of breach or the breach mechanics, the physical model studies are urgently needed to improve and push the breach model development. Large scale physical model and/ or prototype tests are the only tools to solve the breach model's bottleneck.

2. Research Objectives

The main research objective is to investigate the mechanism of the breach growth in cohesive embankments and model the process of the breach growth in the cohesive embankments in the methodology of Energy Theory, Hydraulics, River Mechanics, Soil Mechanics and the Acceptable Risk Analysis as well. The detailed research objectives in the flume experiments are as follows:

- To get insight into the breach development of cohesive embankment
- To clarify the roles of headcut erosion (formation and migration) in the deepening process of the breach (Zhao, et al, 2013)
- To clarify the roles of lateral (helicoidal) erosion in widening process of the breach
- To study the scour hole development downstream the breach
- To study the influence of the initial trench's location on the breaching process
- To compare the lab experiment and field experiment and make clear the scale factors

Physical model is a useful and popular tool to investigate the breaching process in the embankment and has been applied by the former researchers (Visser, 1998; Zhu, 2006) in the laboratory, however, the scale limitations increase the uncertainty of the breaching development and the result distortions have been generated. In the meantime, researchers use prototype data analyses and conduct the real embankment breach tests in the field to get insights into the mechanism of breach development. But the data collected from prototype are usually not complete. The measurement accuracy is not high enough with the field experiments and the costs are much higher than physical model in the laboratory.

In order to reduce the scale impacts and defects of the prototype experiments, the large scale sediment models in the flume are desingned to investigate the embankment breaching process, including surface erosion, headcut erosion and laterial erosion (helicoidal erosion). The breach hydrological process and topography changes are also measured in these experiments.

3 Experiment Design and Setup

3.1 Introduction of the Flume

The 5 runs of experiments were conducted in the flume of 60 m × 3 m × 3 m of Changjiang River Scientific Research Institute, Changjiang River Water Resources Commission, China. The maximum discharge that can be supplied is 1 m^3/s. The flume layouts are shown in Fig. 3, Fig. 4 and Fig. 5. Two sidewall of the flume were made up of forced concrete frame and forced glass, and the transit channel and outlet channel were built with bricks. There are 14 glasses in the main test reach with a total length of 35 m.

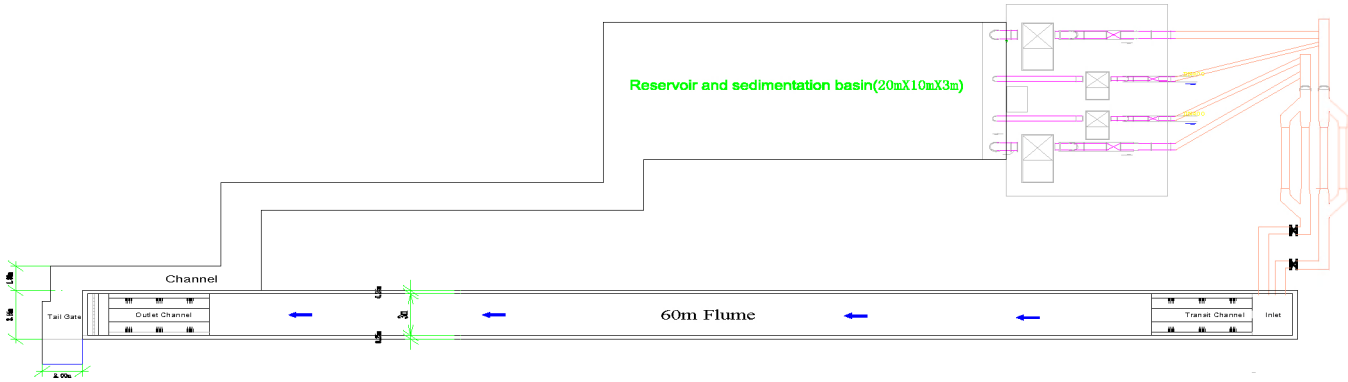

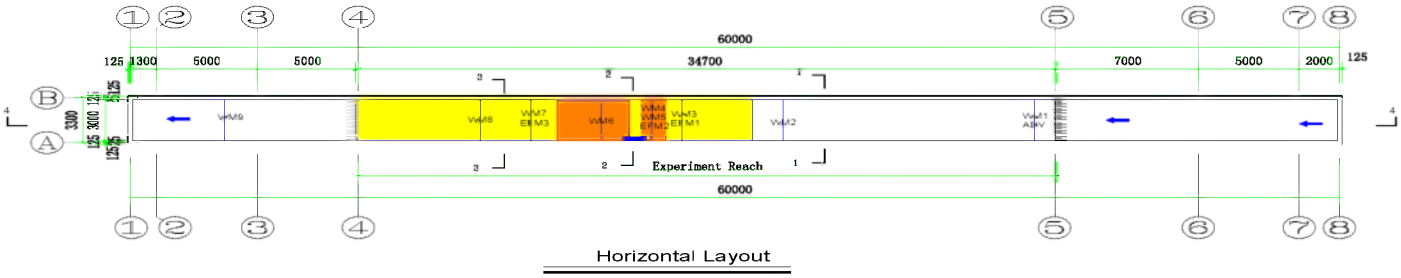

Horizontal Layout

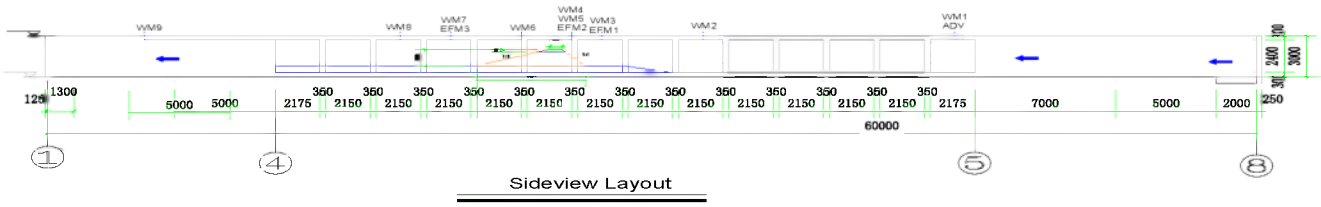

Sideview Layout

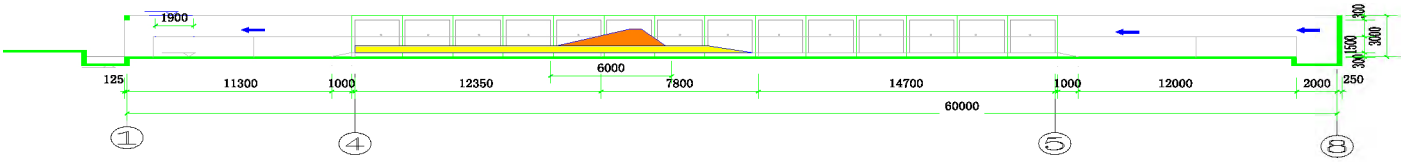

4-4

Figure 3 Layout of the flume

Figure 4 Flume Overview

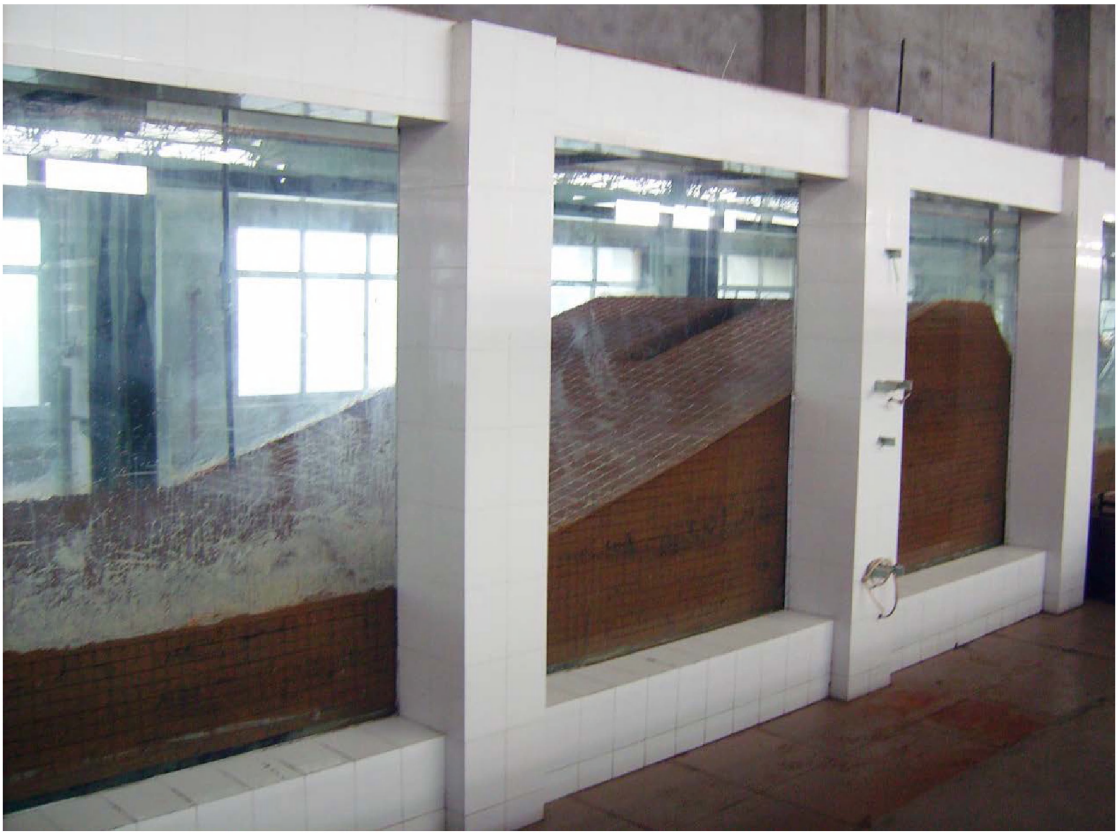

Figure 5 Flume Side View(Model 5)

In the flume system, there are a reservoir and a sedimentation basin to supply the flow and deposit the sediment in the basin (see Fig. 6). It is 20m long, 10m wide and 3m deep. The

discharge is generated by 7 pumps (see Fig. 7) and controlled by two electromagnetic flow meters (see Fig. 8).

Figure 6 Sediment Basin and Reservoir

Figure 7 Flume Pumps Layout

Figure 8 Flume Discharge Meter (Electromagnetic Flow Meter)

3.2 Embankment Model Design

There are 5 runs of experiments in the flume. All the model parameters are show in Table 1, Fig. 9, Fig. 10, Fig. 11, Fig. 12and Fig. 13. The embankments are built on erodible flume bed, 0.8m thick of clay with the same characteristics as the dike. There are four embankments designed of 1.20 m high and one embankment designed of 0.6 m high to study the scale influence. All the riverside slopes are the same in 5 models, i.e., 1:1. The landside slopes are designed of 1:3 and 1:2 to study the influence of the landside slope. And the crest width is designed into 0.6 m. The initial trench is set to 0.5 m wide and 0.2 m deep, with a slope of 1:1.

Table 1 Breach Scale Model Parameters

Parameters	Model 1	Model 2	Model 3	Model 4	Model 5
Experiment Date	01/02/2013	27/02/2013	07/03/2013	14/03/2013	22/03/2013
Initial Trench Location	Side	Side	Side	Side	Middle
Dam Length(m)	3	3	3	3	3
Dam Height(m)	0.6	1.2	1.2	1.2	1.2
Dam Crest Width(m)	0.6	0.6	0.6	0.6	0.6
Riverside slope	1V:1H	1V:1H	1V:1H	1V:1H	1V:1H
Landside slope	1V:2H	1V:2H	1V:3H	1V:3H	1V:3H
Bottom Width (m)	3.6	4.2	4	4	4
Flume bed Length(m)	20	20	20	20	20
Flume bed Thickness(m)	0.5	0.5	0.5	0.5	0.5
Volume(m^3)	33.78	38.64	40.8	40.8	40.8

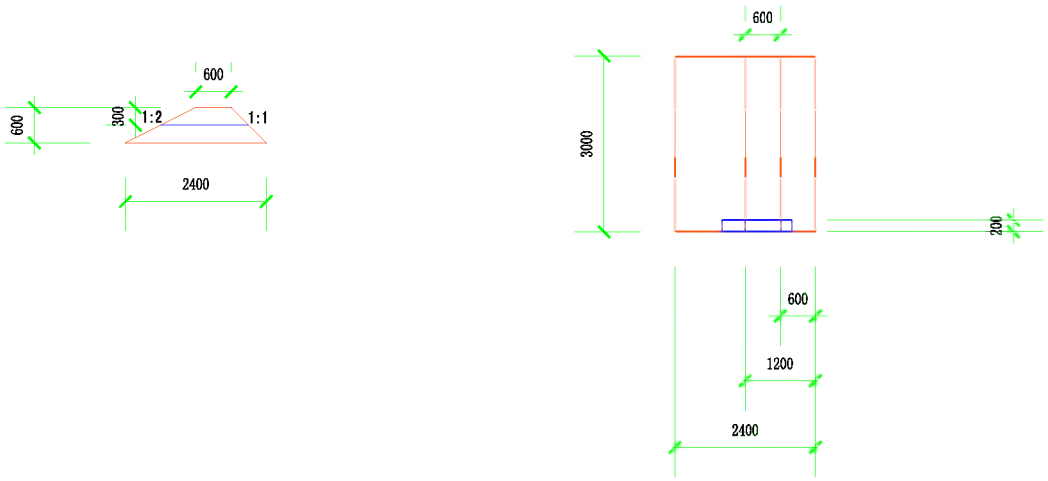

Figure 9 Design of Model 1

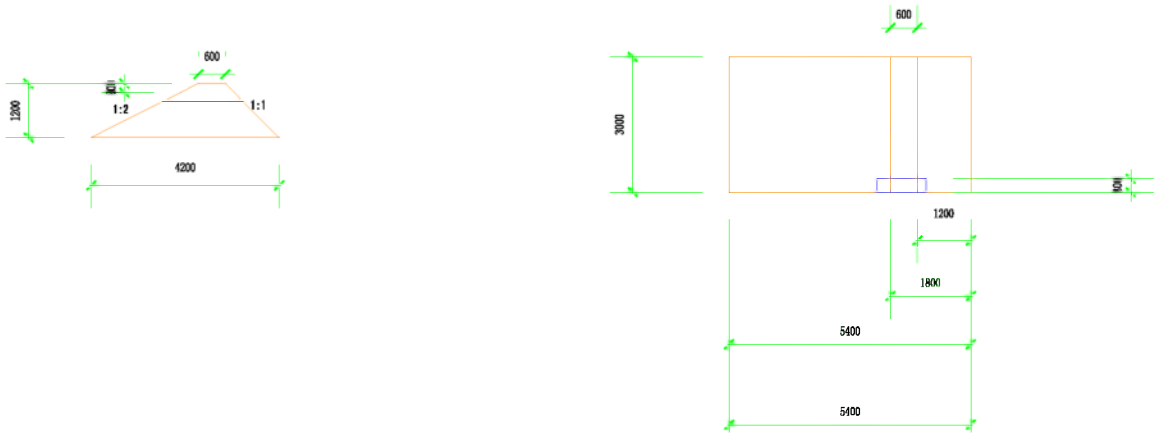

Figure 10 Design of Model 2

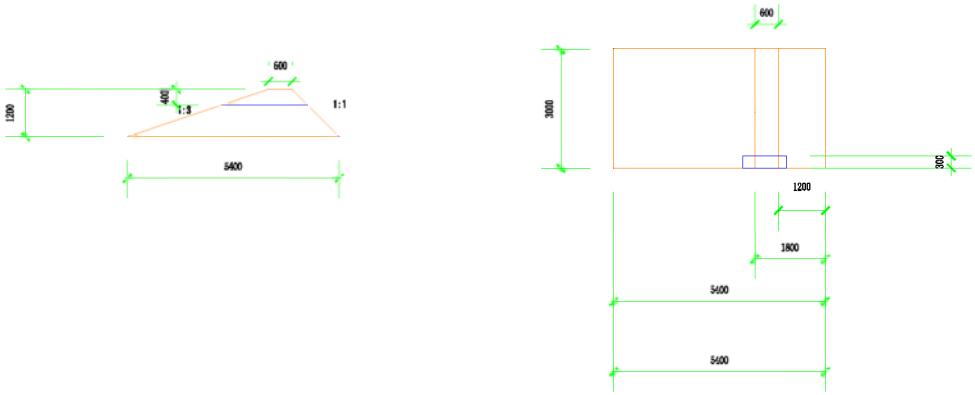

Figure 11 Design of Model 3

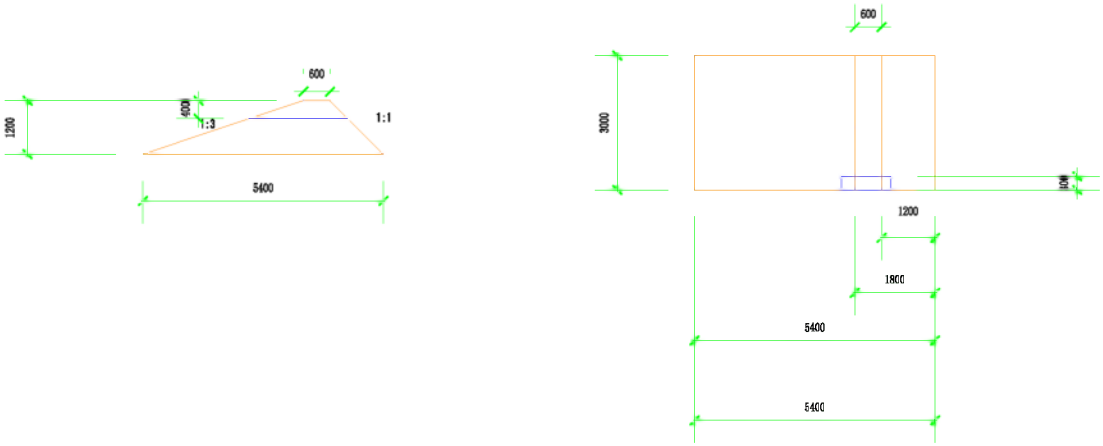

Figure 12 Design of Model 4

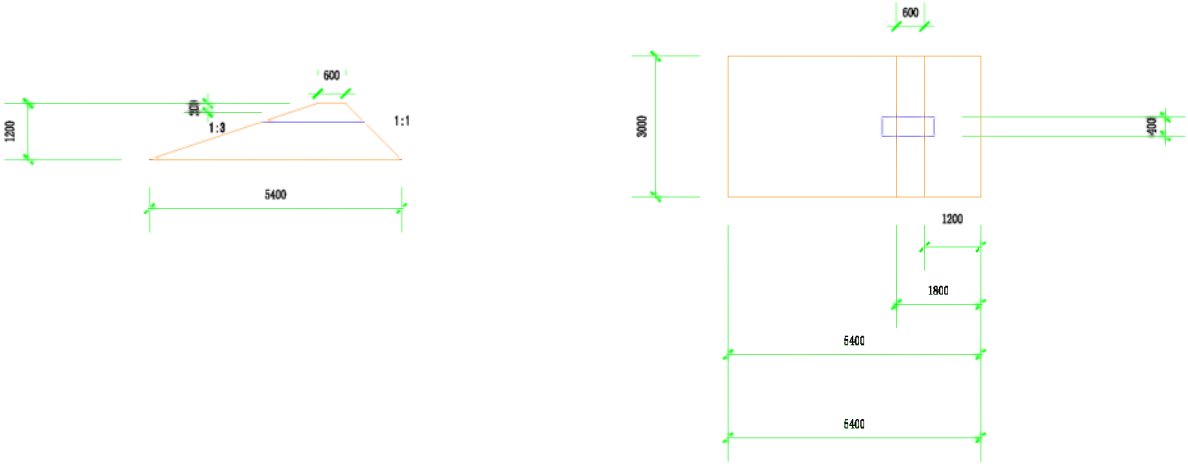

Figure 13 Design of Model 5

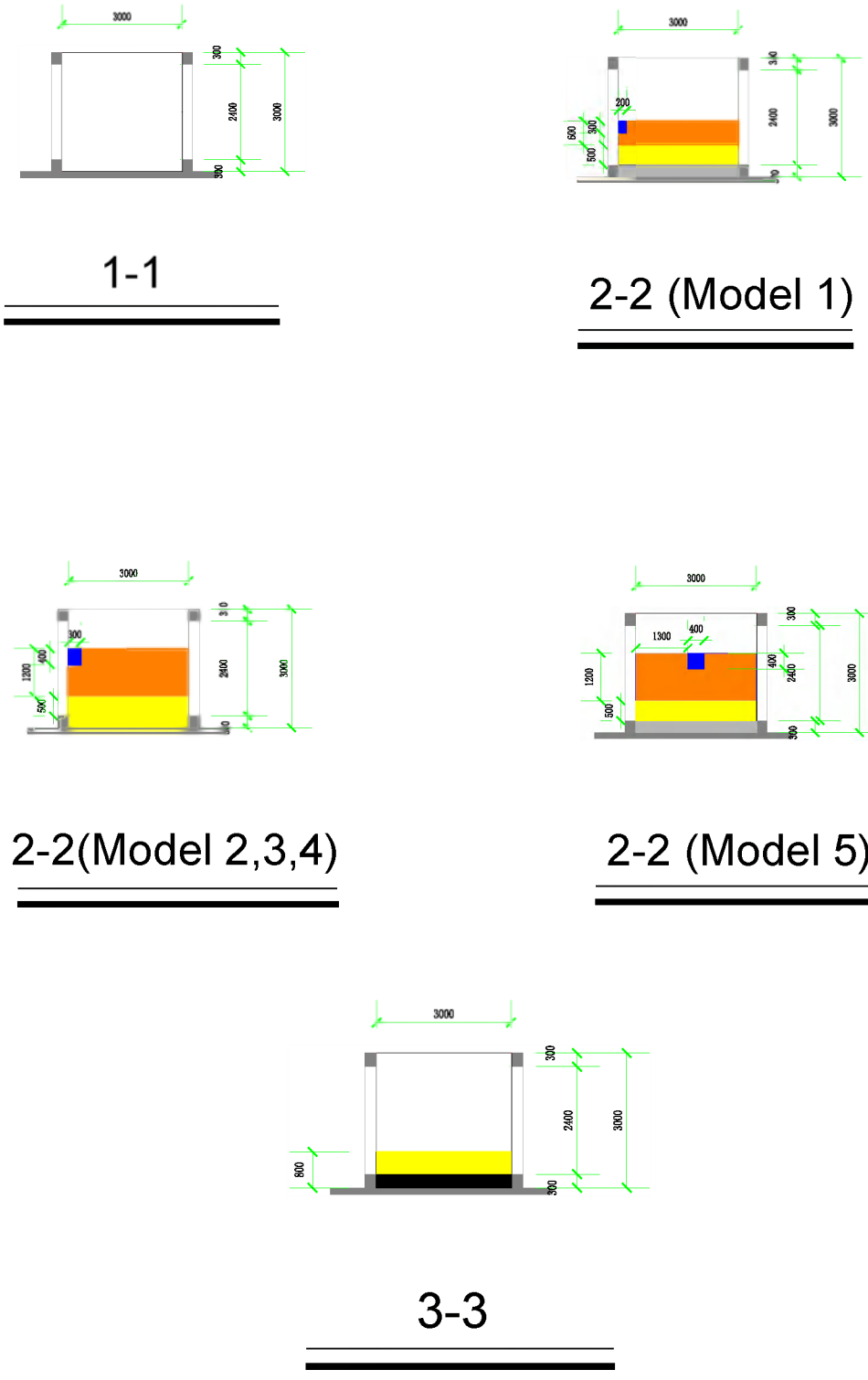

Figure 14 Cross-section (Side Breach; Middle Breach)

In order to study the impact of initial breach location, the models were designed two types of initial breach, side breach (Fig. 14 , Fig. 15) and middle breach (Fig. 14 , Fig. 16). The initial

breach channel is the triggering force to the breach process, i.e., in practice, it is the weakest point in the embankment.

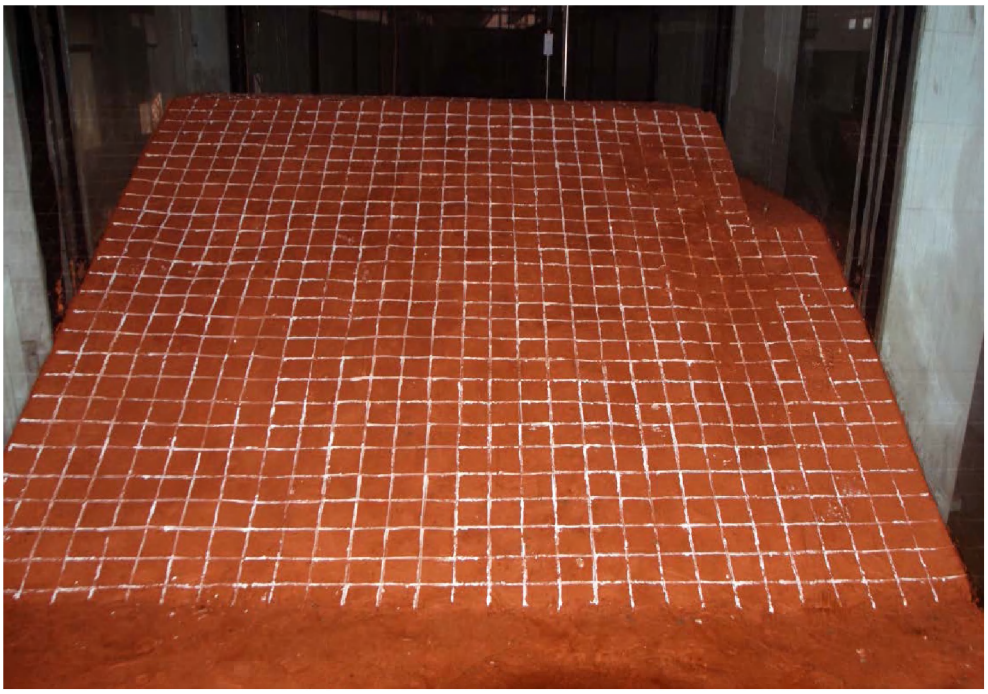

Figure 15 Photo of Model 2

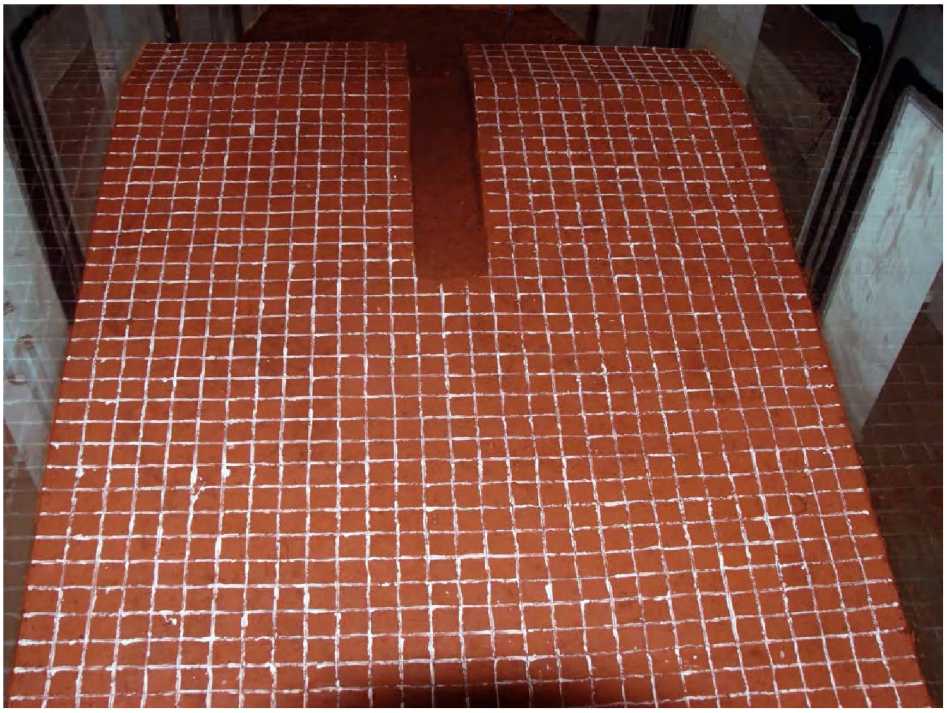

Figure 16 Photo of Model 5

4 Measurement Instrumentation

In the breach process of cohesive embankment, the morphological change depends on the hydraulic parameters; conversely, the morphology influences the hydraulic parameters. Therefore the hydraulic parameters and morphological parameters both play an important role in the breach process. In the flume experiments, the hydraulic parameters, including water level and velocity, are measured with the equipment. And topography is measured with Three dimensional Survey instrument and video cameras.

4.1 Water Level

Water level meters (see Fig. 17) are set on the flume to measure the water level process in the breach. There are 8 water level meters setup along the flume from the inlet channel to the tailgate. In the upstream 4 meters are fixed to measure the water level change process of the reservoir of the embankment. 2 meters are used to measure the embankment breach process just above the crest of the embankment and in the initial channel of the embankment. In the downstream of the embankment, there are meters to measure the water level process and control the tailgate water level.

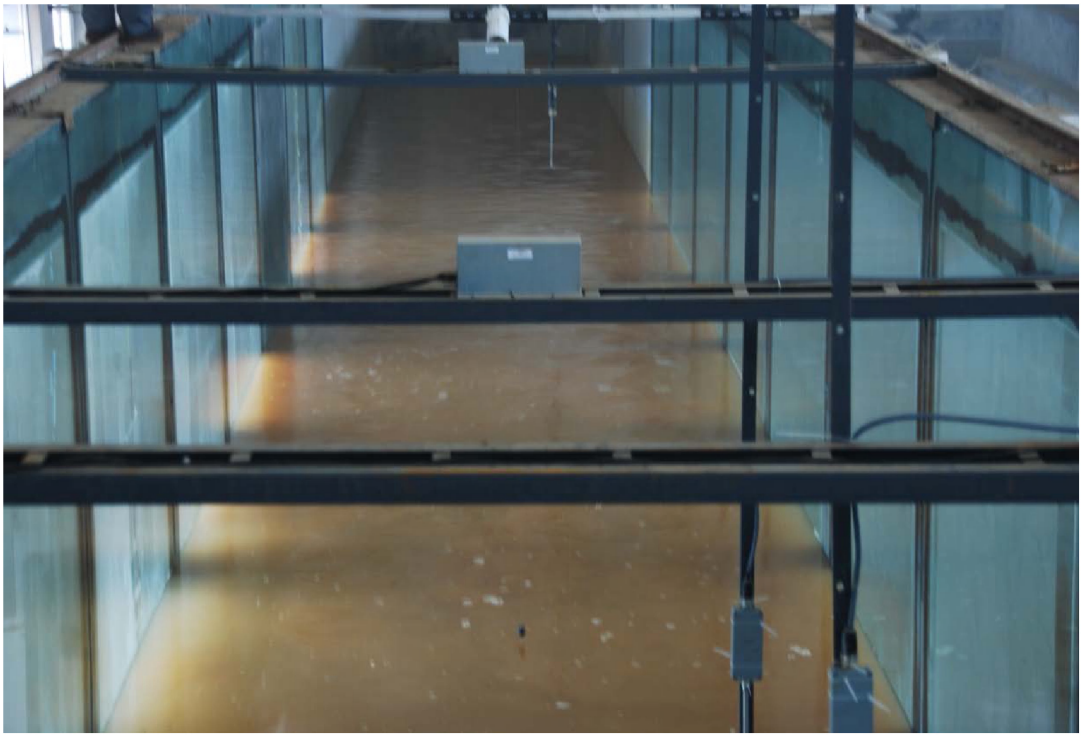

Figure 17 Water Level Meter

4.2 Velocity

3 Electromagnetic Velocity Meters (see Fig. 18) were fixed upstream of the breach, in the breach channel and downstream of the breach to measure the flow velocity process, respectively. Particle trace was used to indicate the velocity distribution at the flow surface while the 3 High-speed video camera systems recorded the breaching process. According to the video records, the surface velocity could be measured and calculated using the trace particle movements.

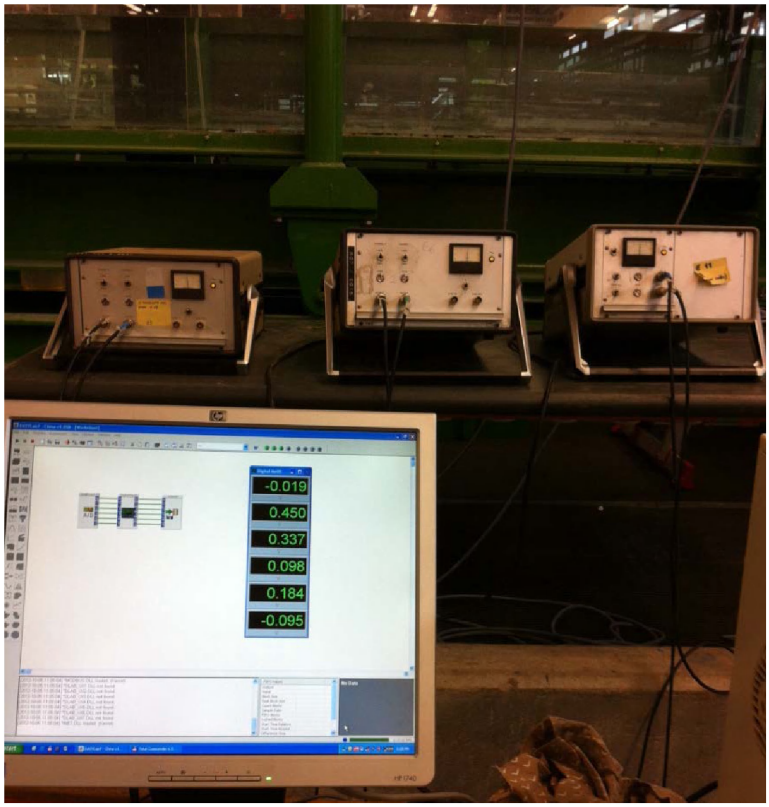

Figure 18 Electromagnetic Velocity Meter System

4.3Topography

Topography Survey Instrument is used to measure the embankment topography variation every 5 minutes. A three Dimensional Laser Scanner (see Fig. 19) is used to measure the breach geometry variation. Video Cameras were fixed above the breach to record the breach process. The scour hole and breach channel development were measured and recorded with topography survey instruments and video camera through the glass wall of the flume.

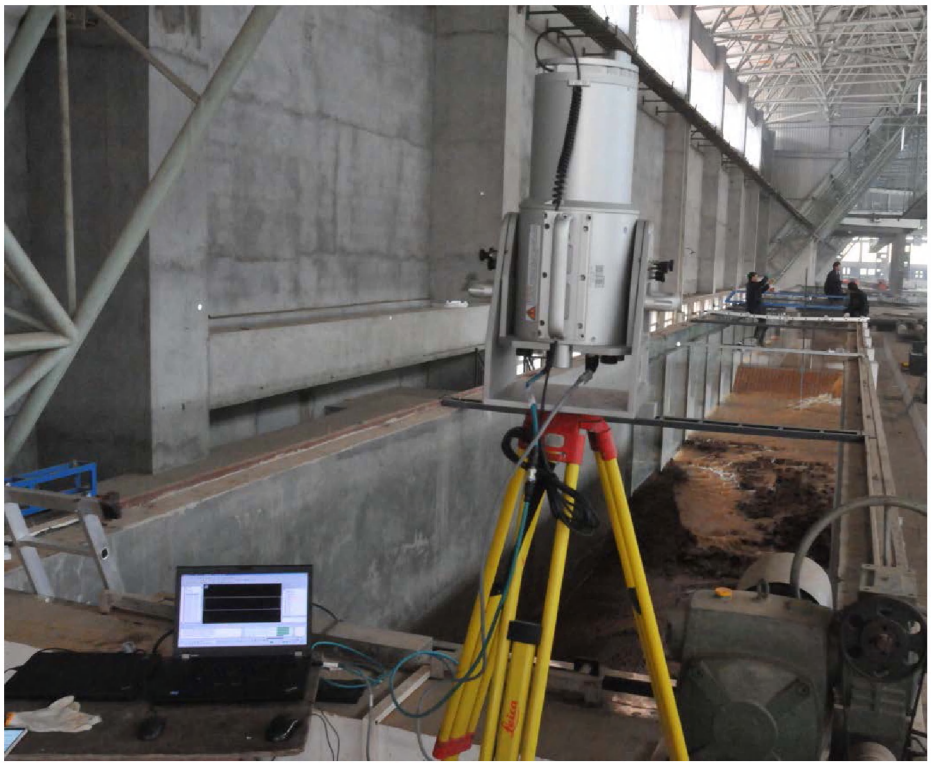

Figure 19 Three Dimensional Laser Scanner Systems

5 Soil Test

5.1 Soil Collection

The embankment material is the mixture of clay and silt collected and delivered from Houguanhu Lake bank. The excavator (see Fig. 20) was used to pick up the clay from the site to the trucks.

In total 41 truckloads of soil were delivered to the experiment hall which is more than 2,000 m^2 for reproduction. The total amount of soil was more than 125 m^3. The soil (see Fig. 21) was first transported to the experiment hall and then paved to a layer of 10 cm by the workers.

Figure 20 Excavator and Truck in the delivery

Figure 21 Soil paved in the experiment hall

5.2 Soil Reproduction

After 20 days in the air, the soil was dry and re-produced to a small diameter of block from the natural size (see Fig. 22). The maximum size of re-produced soil was controlled to be less than 5 cm.

Figure 22 Re-produced Soil

In order to build the model easily with the soil, the dried soil was reproduced again by the grinder (see Fig. 23) into finer size. The controlled diameter is 1.5 cm and the fine soil was shown in Fig. 24. It is suitable to reproduce into any size used in the model construction.

Figure 23 Grinder to reproduce the soil

Figure 24 Re-produced fine soil

As for the model construction, a suitable water content and soil size were requested. The blender (see Fig. 25) was used to adjust the soil water content and mix the clay sample homogenously.

Figure 25 Blender to reproduce the soil sample

5.3 Soil Test in the lab

Cohesive embankment breaching is a hydraulic phenomenon coupled with soil mechanics. So a series of soil tests in the lab were conducted before the flume experiments were conducted. A wide variety of laboratory tests can be performed on soils to measure a wide variety of soil

properties. Some soil properties are intrinsic to the composition of the soil matrix and are not affected by sample disturbance, while other properties depend on the structure of the soil as well as its composition, and can only be effectively tested on relatively undisturbed samples. Some soil tests measure direct properties of the soil, while others measure "index properties" which provide useful information about the soil without directly measuring the property desired.

Soil tests in the laboratory concerned in this breaching experiment contains water content, density (dry density, relative density), particle size analysis, proctor compaction test, Atterberg limits (shrinkage limit, plastic limit, liquidity limit), direct shear stress, triaxial shear test, permeability, and compression.

5.3.1 Density and Water Content

In order to keep the embankment homogenous, the models were made layer by layer, each layer having a thickness of 20 cm. And the samples were collected after every layer had been compressed. Then the bulk density, dry density and water content were tested in the soil mechanics laboratory. The bulk density distributions were shown in Fig. 26. The bulk density distributions in the 5 models had small differences, and in the construction error ranges. The dry densities (Fig. 27) also have well homogenous distributions. Water content tests (Fig. 28) provide the water content of the soil, normally expressed as a percentage of the weight of water to the dry weight of the soil. It can impact the cohesion of the model material.

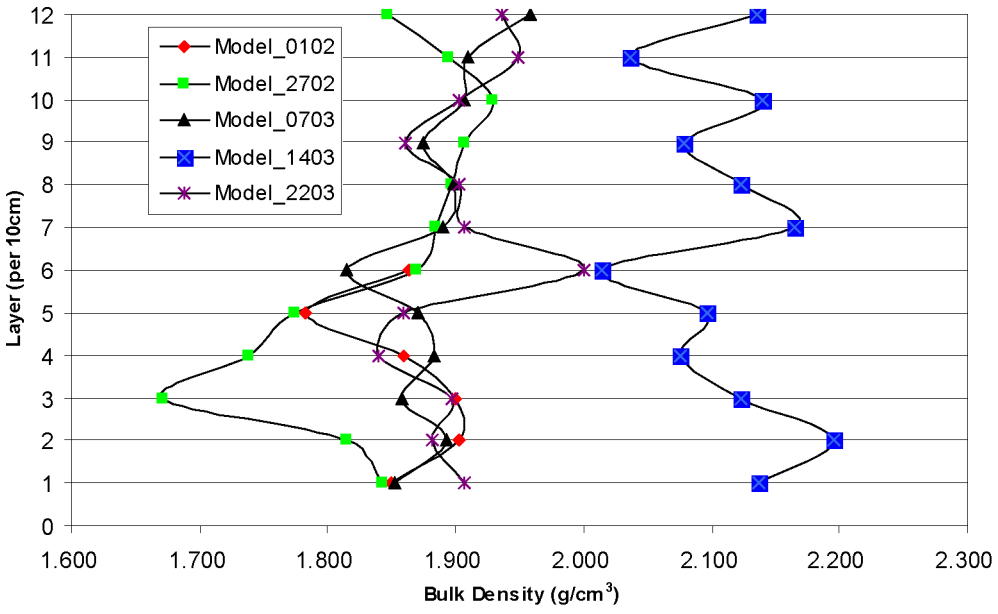

Figure 26 Model Material Bulk Density Distributions

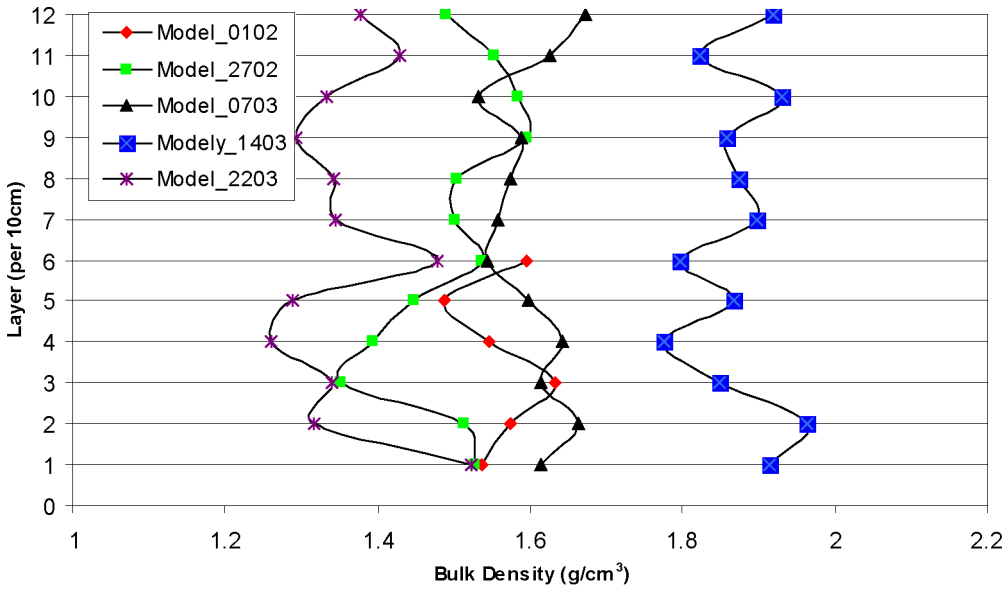

Figure 27 Model Material Dry Density Distributions

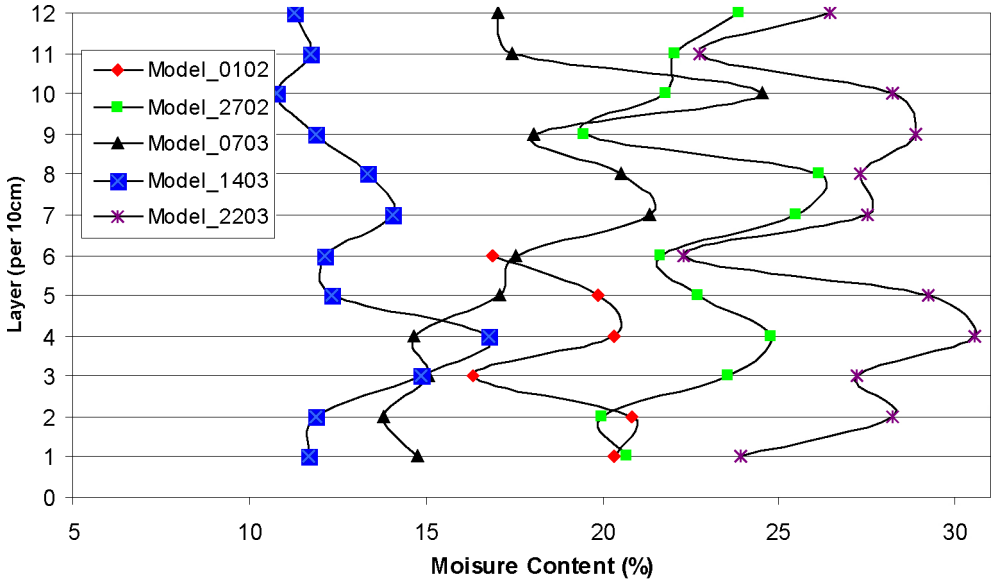

Figure 28 Model Material Bulk Density Distributions

5.3.2 Particle Size Analysis

Particle size analysis is done to determine the soil gradation. Coarser particles are separated in the sieve analysis portion, and the finer particles are analyzed with a hydrometer. The distinction between coarse and fine particles is usually made at 75 μm. The sieve analysis shakes the sample through progressively smaller meshes to determine its gradation. The hydrometer analysis uses the rate of sedimentation to determine particle gradation (see Fig. 29). The sand-clay mixture was used to build model 4.

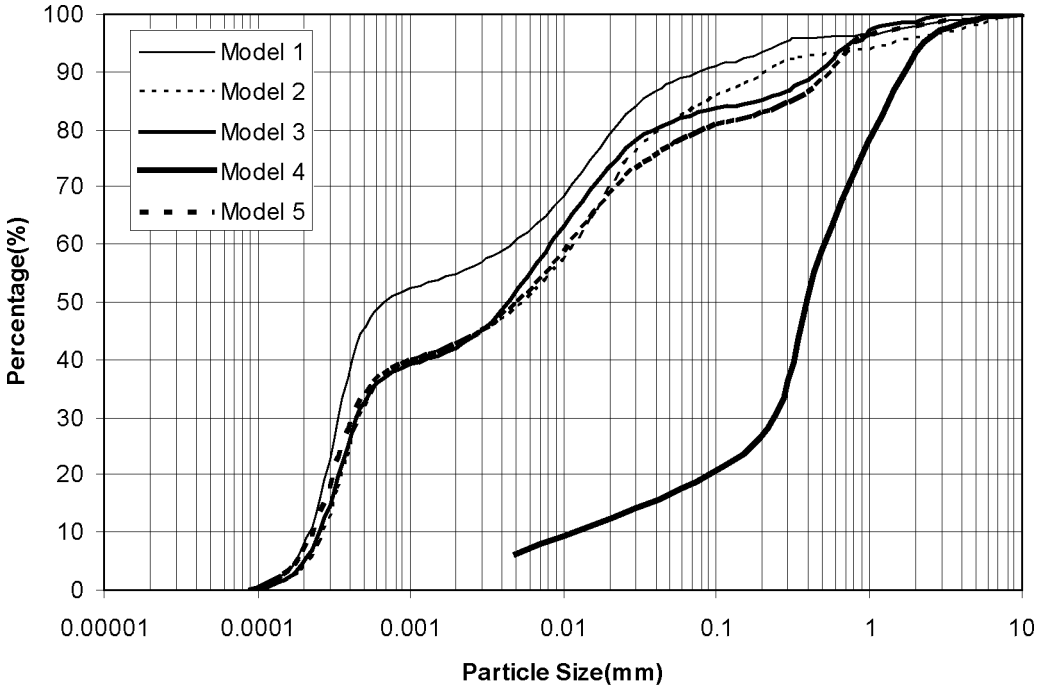

Figure 29 Model material grading

5.3.3 Proctor Compaction Test

Compaction is the process by which the bulk density of an aggregate of matter is increased by driving out air. For any soil, for a given amount of compactive effort, the density obtained depends on the moisture content. At very high moisture contents, the maximum dry density is achieved when the soil is compacted to nearly saturation, where (almost) all the air is driven out. At low moisture contents, the soil particles interfere with each other; addition of some moisture will allow greater bulk densities, with a peak density where this effect begins to be counteracted by the saturation of the soil.

According to the proctor compaction test process, 4 clay samples (without Model 4) were prepared with different compaction times. The relationships (see Fig. 30) between optimum water content and dry density were obtained after 5 times of compactions. The optimum water content is 21.3% and the maximum dry density is 1.61g/m^3 based on the compaction tests.

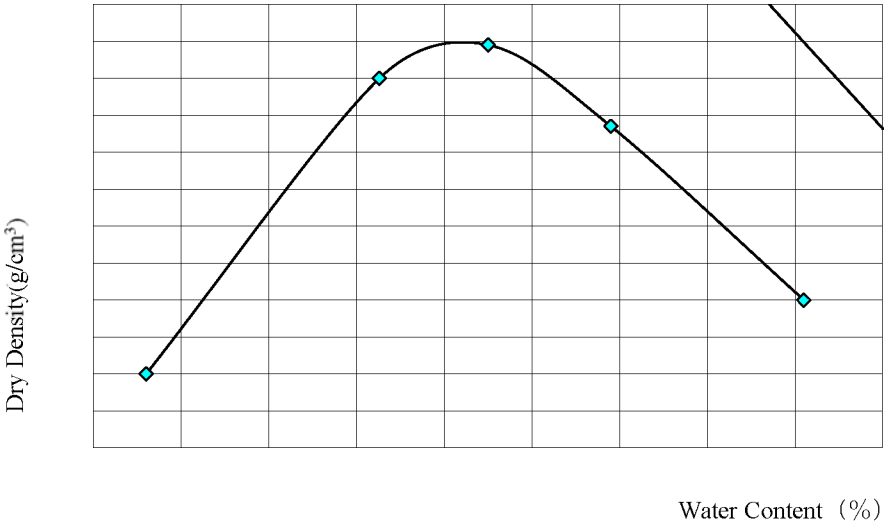

Figure 30 Relationship between Optimum Water Content and Dry Density

5.3.4 Atterberg Limits

The Atterberg limits are a basic measure of the nature of a fine-grained soil. Depending on the water content of the soil, it may appear in four states: solid, semi-solid, plastic and liquid. In each state the consistency and behavior of a soil is different and thus so are its engineering properties. Thus, the boundary between each state can be defined based on a change in the soil's behavior. The Atterberg limits can be used to distinguish between silt and clay, and it can distinguish between different types of silts and clays. The Atterberg Limits test results are shown in Table 2.

(1) Shrinkage limit

The shrinkage limit (SL) is the water content where further loss of moisture will not result in any more volume reduction. The test to determine the shrinkage limit is ASTM International D4943. The shrinkage limit is much less commonly used than the liquid and plastic limits.

(2) Plastic limit

The plastic limit is determined by rolling out a thread of the fine portion of a soil on a flat, non-porous surface. The procedure is defined in ASTM Standard D 4318. If the soil is plastic, this thread will retain its shape down to a very narrow diameter. The sample can then be remolded and the test repeated.

As the moisture content falls due to evaporation, the thread will begin to break apart at larger diameters. The plastic limit is defined as the moisture content where the thread breaks apart at a diameter of 3 mm.

(3) Liquid limit

The liquid limit (LL) is the water content at which a soil changes from plastic to liquid behavior. The original liquid limit test of Atterberg's involved mixing a part of clay in a round-bottomed porcelain bowl of 10-12cm diameter. A groove was cut through the pat of clay with a spatula, and the bowl was then struck many times against the palm of one hand.

Table 2 Atterberg Limits test results

liquid limit (LL)	liquid limit (LL)	Plastic limit	Plasticity Index	Plasticity Index
W_{L17}	W_{L10}	W_p	I_{P17}	I_{P10}
%				
48.3	38.6	19.6	28.7	19.0

5.3.5 Direct Shear Stress

The direct shear test determines the consolidated, drained strength properties of a sample. A constant strain rate is applied to a single shear plane under a normal load, and the load response is measured. If this test is performed with different normal loads, the common shear strength parameters can be determined (see Table 3).

5.3.6 Triaxial Shear Test

This is a type of test that is used to determine the shear strength properties of a soil. It can simulate the confining pressure a soil would see deep into the ground. It can also simulate drained and undrained conditions.

The unconsolidated undrained tests were used to test Zhuankou clay sample. In the test, the sample is not allowed to drain. The shear characteristics are measured under undrained conditions and the sample is assumed to be unsaturated. Figure 28 shows the relationships between stress and strain under the pressure of 50 kPa, 100 kpa and 150 kPa. Based on the Mohr's strain circle method, the triaxial shear test result are shown in Table 3.

Table 3 Model Sample Characteristics

NO.	Sample	Soil Type	Sample Characteristics			
			Moisture content	Bulk density	dry density	Degree of saturation
			w	ρ	ρ_d	Sr
			%	g/cm^3	g/cm^3	%
1	Model 1	silty clay	28.8	1.86	1.47	92.6
2	Model 2	silty clay loam	28.7	1.84	1.49	94.8
3	Model 3	silty clay	26	1.88	1.51	86.5
4	Model 4	loam sand	16.1	2.11	1.84	93.2
5	Model 5	silty clay	26.4	1.90	1.54	93.7
6	Model Layer	silty clay loam	29.5	2.01	1.48	90

Table 3 Model Sample Characteristics (continued)

NO.	Mechanic Indicator						Permeability test
	Compression test		Direct shear stress		Triaxial shear test(UU)		
	a_{v1-2}	Es_{1-2}	C_q	φ_q	C_u	φ_u	K_{20}
	MPa^{-1}	MPa	kPa	°	kPa	°	cm/s
1	0.322	6	14	3.6	12.7	3.0	8.02E-06
2	0.327	5	20.2	1.6	8.1	2.0	7.90E-06
3	0.313	7	19	4.8	16.9	0	50E-06
4	0.082	18.2	8.2	33.6	4.4	32.1	1.36E-04
5	0.254	7.0	16.0	4.2	14.6	6.0	1.75E-05
6	0.312	6.1	16.0	1.9	11.9	1.9	71E-06

5.3.7 Permeability Test

Constant head permeability tests are used to calculate seepage potential through earthen dams and embankments such as dikes. The testing uses a specialized device referred to as a constant head permeameter. In the test, the permeameter is filled with test soil and water run through the sample until the soil is saturated. The amount of water that is discharged from the soil and water mixture in a measured length of time is used as an input to a formula used to determine the soil permeability. The length of time used in the test can vary, but should be consistent during all tests performed for a location. The permeability rate was listed in Table 3 for 5 runs of experiments as well as the clayey layer of the model.

5.3.8 Compression Test

A common method of conducting the test, as described in several published standard test methods, is to compress a box at a constant rate of 12.5 mm per minute between two rigid platens. The platens can be fixed so that they remain parallel or one can be pivoted or "floating". The test can be conducted on empty or filled boxes, with or without a box closure.

After the compression test of Zhuankou clay, the compression factor $av_{1\text{-}2}$ is 0.265 mPa^{-1}, and the compression modulus $Es_{1\text{-}2}$ is 62.30 mPa.

6 Model Tests

There are 5 runs of experiments conducted in the flume (Fig. 2) and the dike models were built according to the designs (see Table 1). Model 1 was conducted February 1, 2013, later Model 2, Model 3, Model 4 and Model 5 were conducted on February 27, March 7, March 14 and March 22, respectively.

6.1 Boundary conditions

The upstream boundary condition for each run of the experiments were controlled by the discharge and water level. The front water level of the embankment was kept in the overtopping condition, i.e., water levels were controlled at 2.00 m for Model 2, Model 3, Model 4 and Model 5, and as for Model 1, the water level was controlled at 1.40 m. In order to control the water semi-constant, the discharge (Fig. 31) was adjusted by the electromagnetic discharge meter.

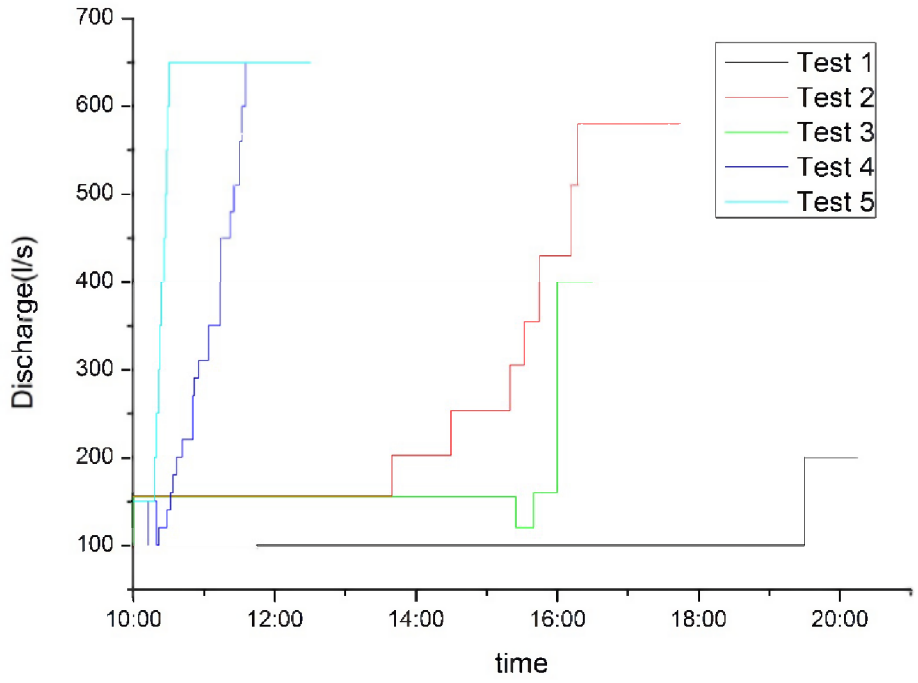

Figure 31 Discharge process for 5 runs of experiments

In each run of the experiments, the water temperatures and sediment concentrations were measured (see Table 4). All the water temperatures were above 10 ℃ and the sediment concentrations increased from 3.739 g/l in the first run of the experiment to 5.000 g/l in the last run of the experiment since the recycled water was stored in the reservoir.

Table 4 Water Temperature and Sediment Concentration

RUN	Water Temperature (℃)	Sediment Concentration (g/l)
EXP_0102	10	3.739
EXP_2702	15	3.884
EXP_0703	13	4.556
EXP_1403	10	4.862
EXP_2203	13	5.000

6.2 Water Level

In the 5 runs of breach experiments, the water levels were measured and recorded upstream and downstream of the model embankment. WM1 measured the controlling water level of the flume. WM4 and WM5 measured the upstream water level close to the embankment crest. The water level processes in the breaching experiments are shown in Fig. 32, Fig. 33, Fig. 34, Fig. 35, Fig. 36.

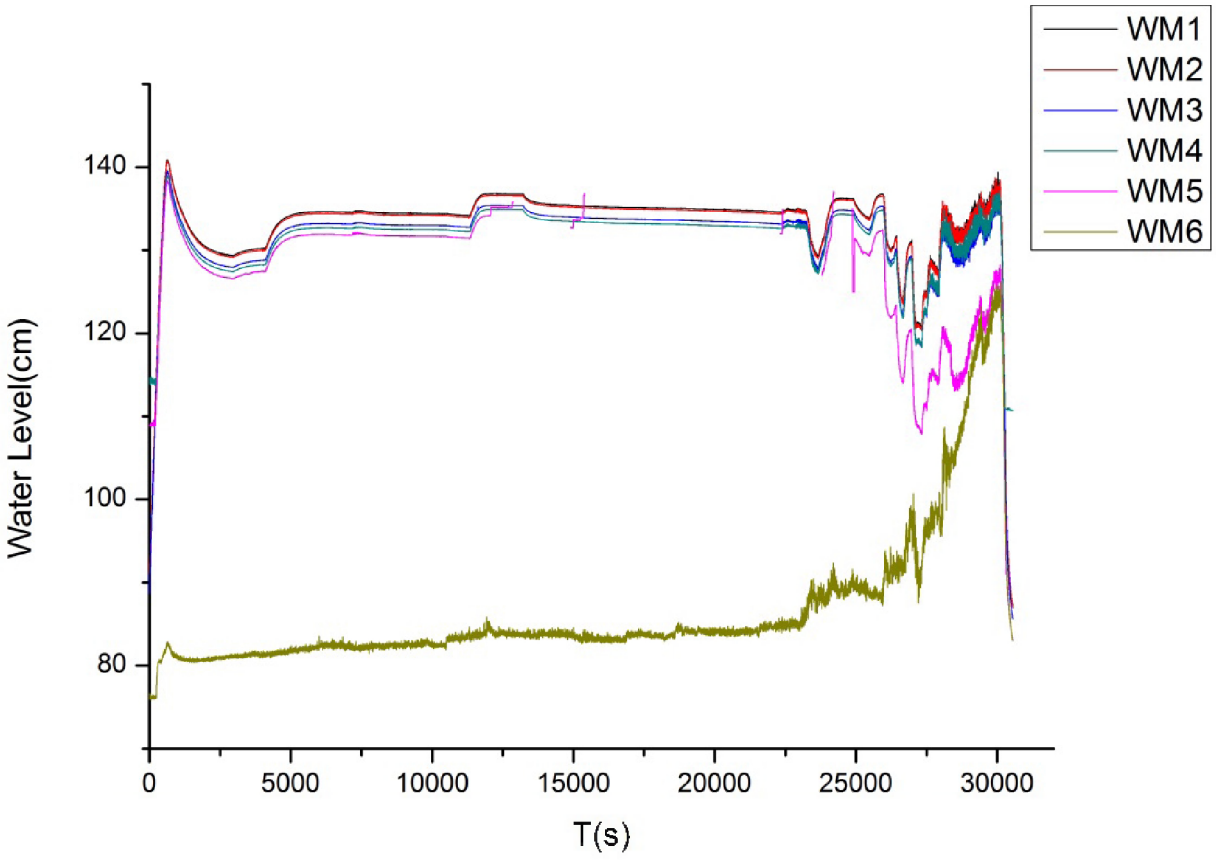

Figure 32 Water Level Process of M1

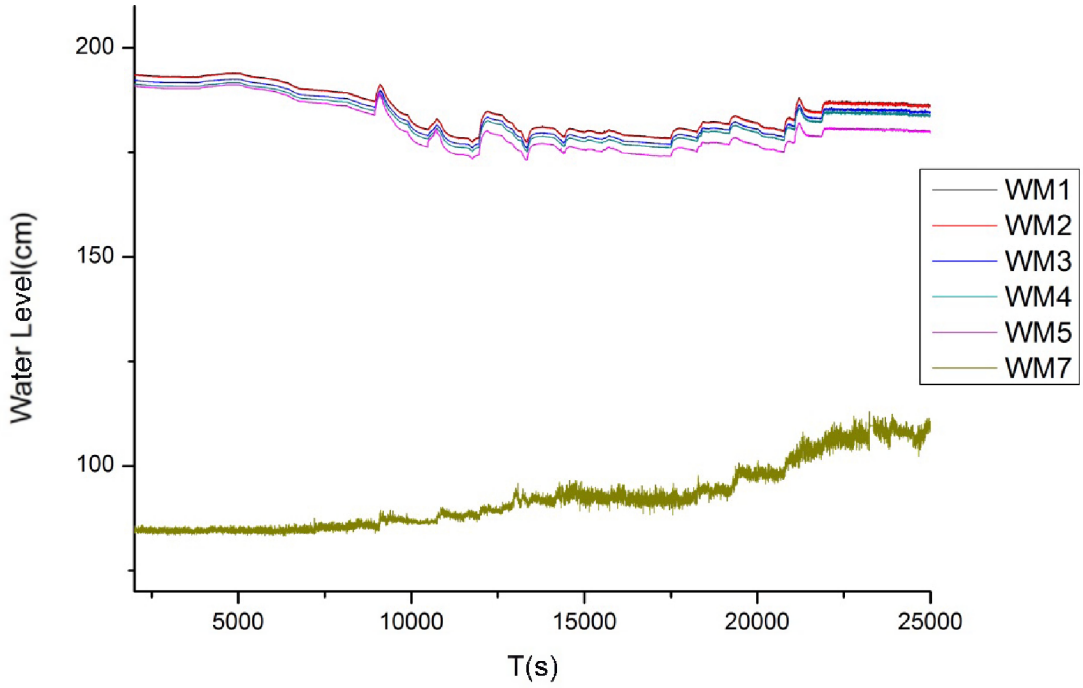

Figure 33 Water Level Process of M2

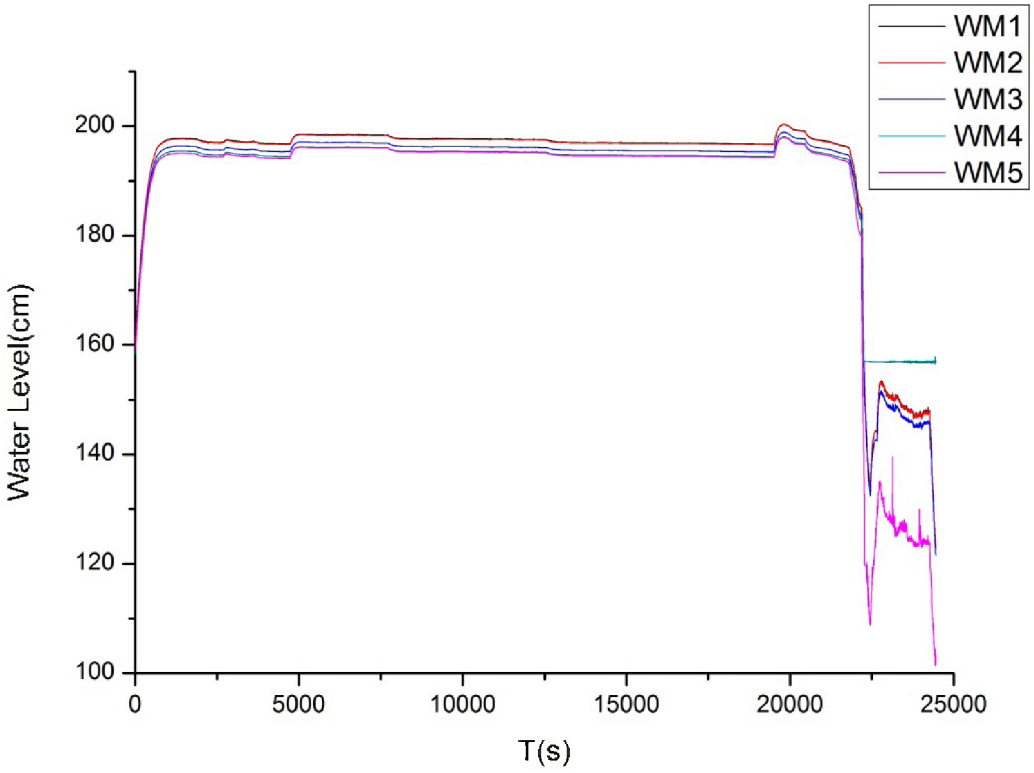

Figure 34 Water Level Process of M3

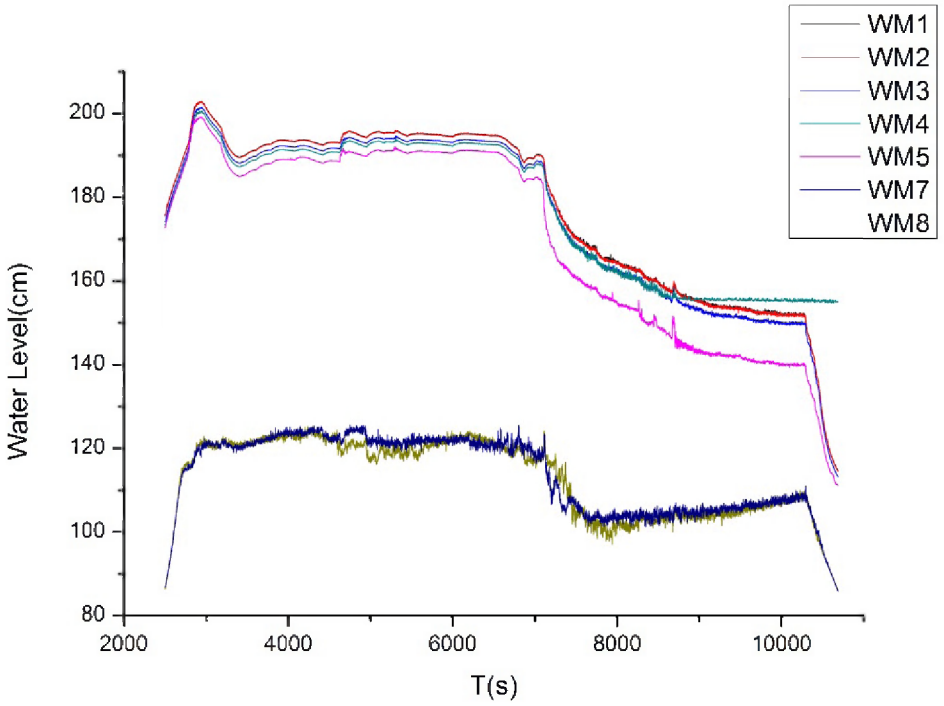

Figure 35 Water Level Process of M4

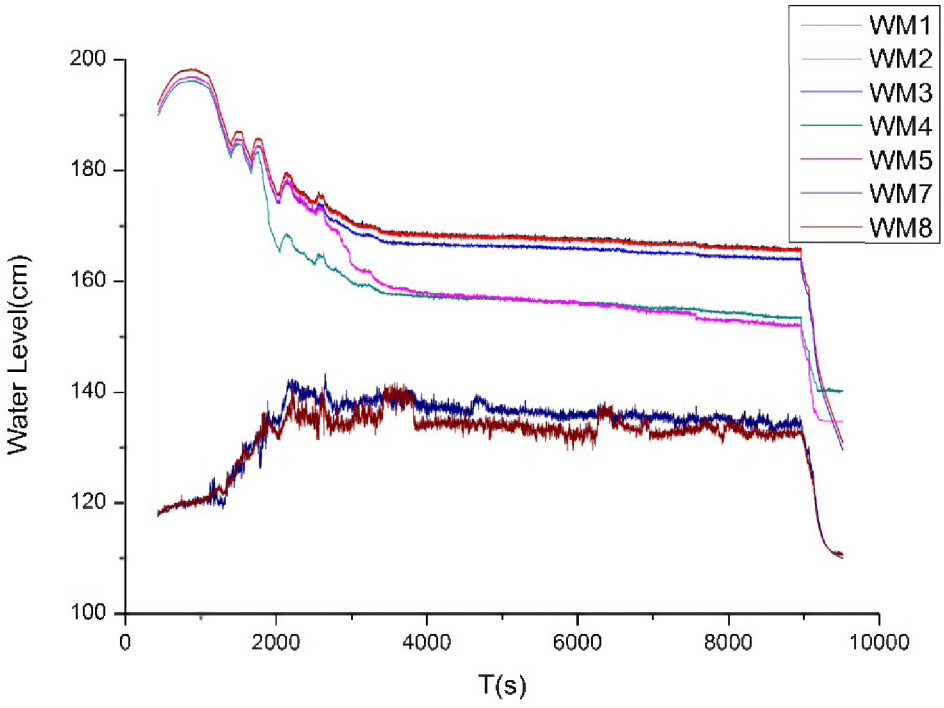

Figure 36 Water Level Process of M5

6.3 Morphological Process in the Breach

Morphological process plays ab important role in the breaching process of cohesive embankments. The change in morphology results from the erosion triggered by the breaching flow. In the study, the morphological process was measured by the 3D scanner every 5 minutes.

Before the experiment started, the total topography of the flume model was scanned (Fig. 37). Model 4 had a side initial breach channel and when the flow came from the upstream and went through the initial channel, the breaching process started via erosion. The surface erosion (Fig. 38) happened due to the flow generated by the high water pressure in the reservoir. The flow firstly broke the embankment surface and washed away the model material by blocks, not by particles.

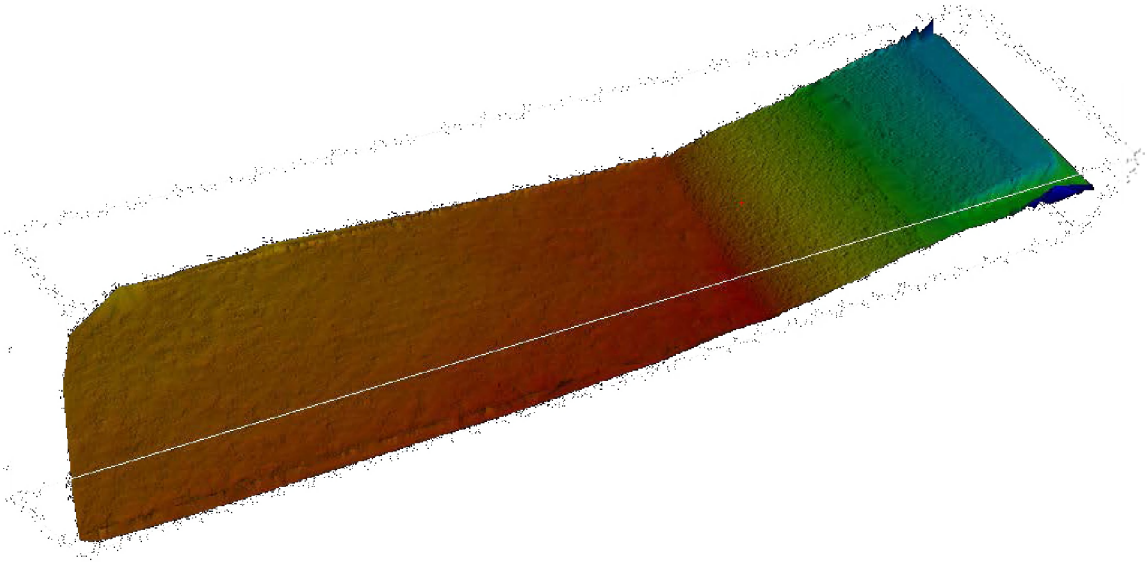

Figure 37 Topography of the model before the test (Run 4)

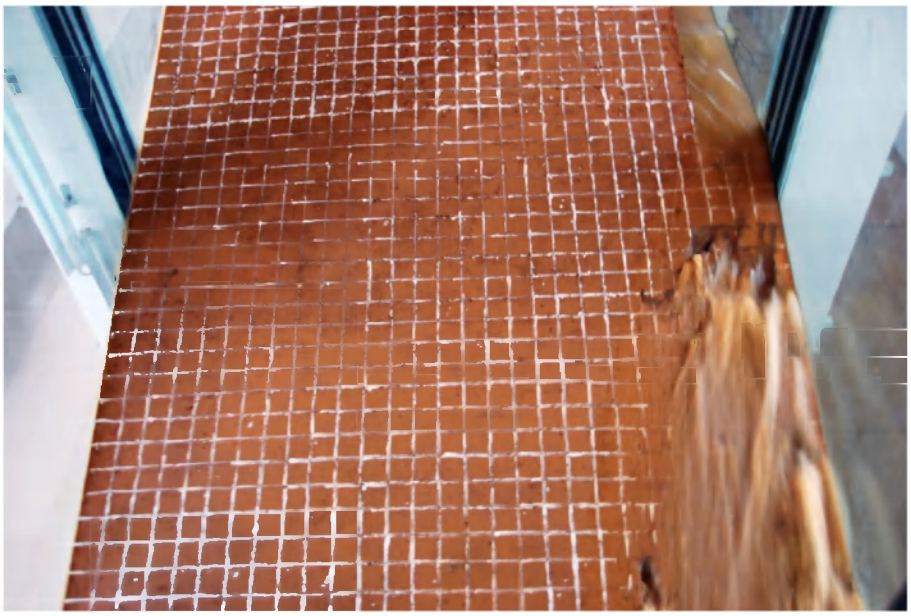

Figure 38 Surface Erosion at the initial phrase of breach

As the development of the breach, the cascade headcut erosion (Fig. 39) started to develop from the toe of the embankment after the fully completion of the surface erosion on the model surface. The blocks of the clay were washed out by the high velocity breaching flow. The initial breach channel (Fig. 40) increased to 1.020 m stimulated by the breaching flow and the embankment toe was fully eroded by the headcut erosion.

Figure 39 Photo of Headcut Erosion

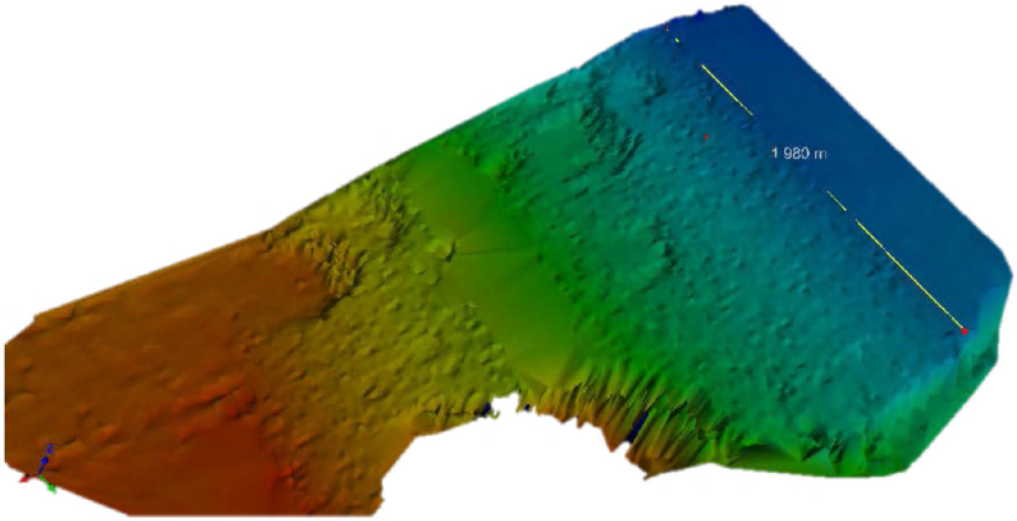

Figure 40 Topography Change during the test (Run 4)

As the development of the headcut erosion processed, the lateral erosion started to play an important role in the breaching process. Due to the helicoidal flow (secondary flow) in the breach channel (Fig. 41), the under mining process triggered the erosion at the side toe of the embankment. The helicoidal erosion at the side toe broke the balance of the embankment and the material blocks collapsed due to the unbalanced situation of the embankment. The helicoidal erosion stimulated the lateral development of the breach channel and made the breach width increase directly. Due to the cohesion of the material, the lateral breach slope (Fig. 42) was generate very steep by the breach flow. The undermining process at the side toe of breach channel usually made the breach slope into negative one.

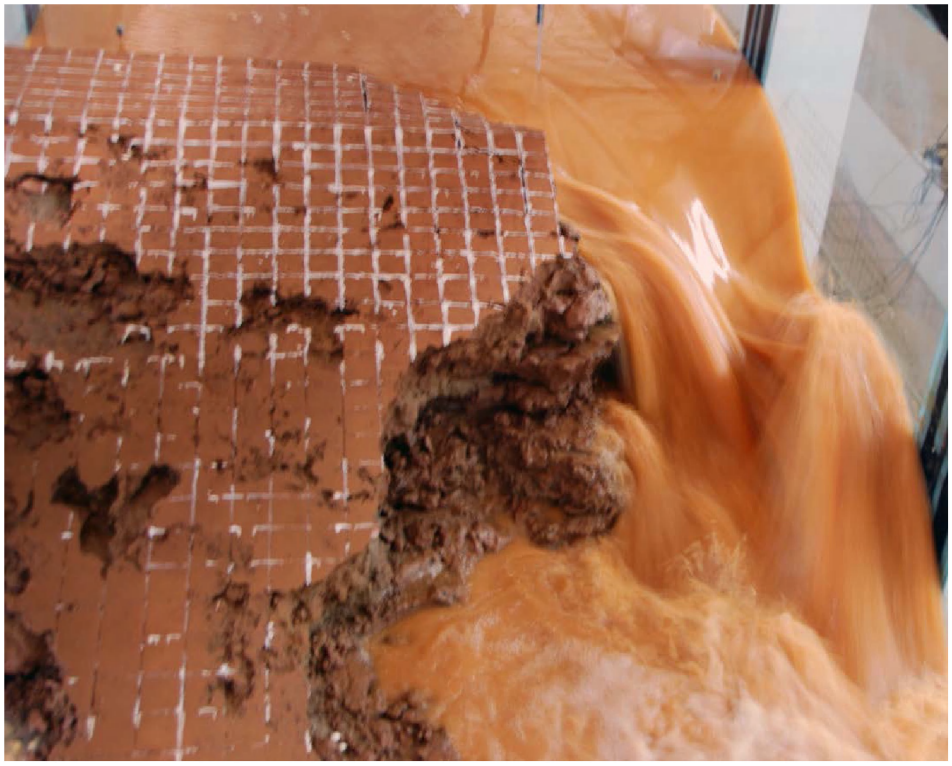

Figure 41 Lateral erosion of the breach

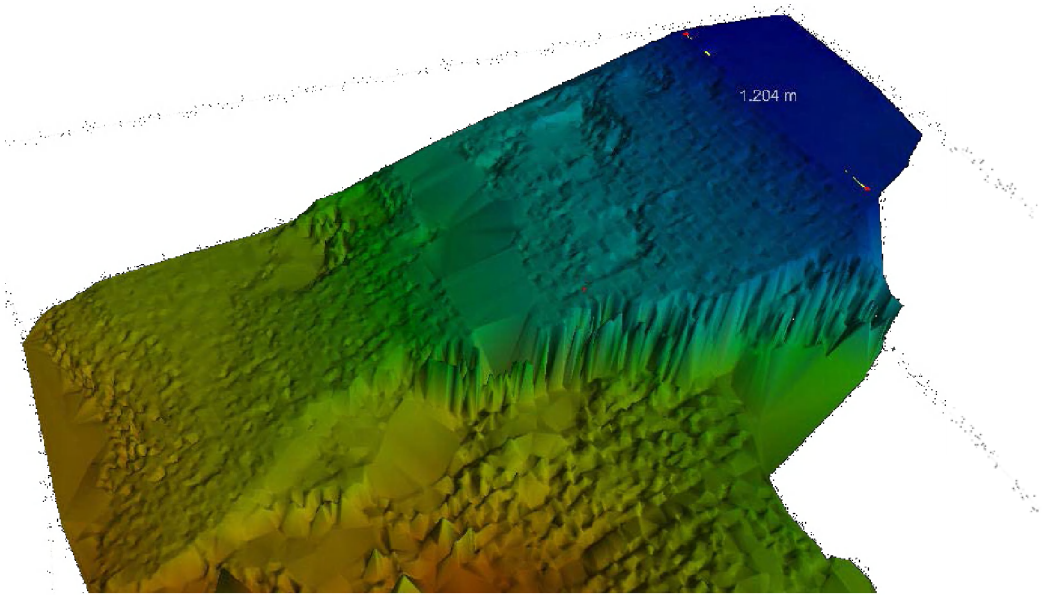

Figure 42 Steep Breach Side Slope

After the initial surface erosion, the embankment breaching process was driven by headcut erosion and helicoidal erosion. Due to the high velocity of the flow through the breach, a

scour hole developed in the breach channel and at the toe of embankment (Fig. 43). The embankment toe scour hole started to form in the early stage of the breaching process, but the eroded material from the embankment covered the scour hole during the following phrases in the breaching. The sour hole formed at the bottom of the embankment in the last phase of the breach and the eroded material was washed away to the downstream.

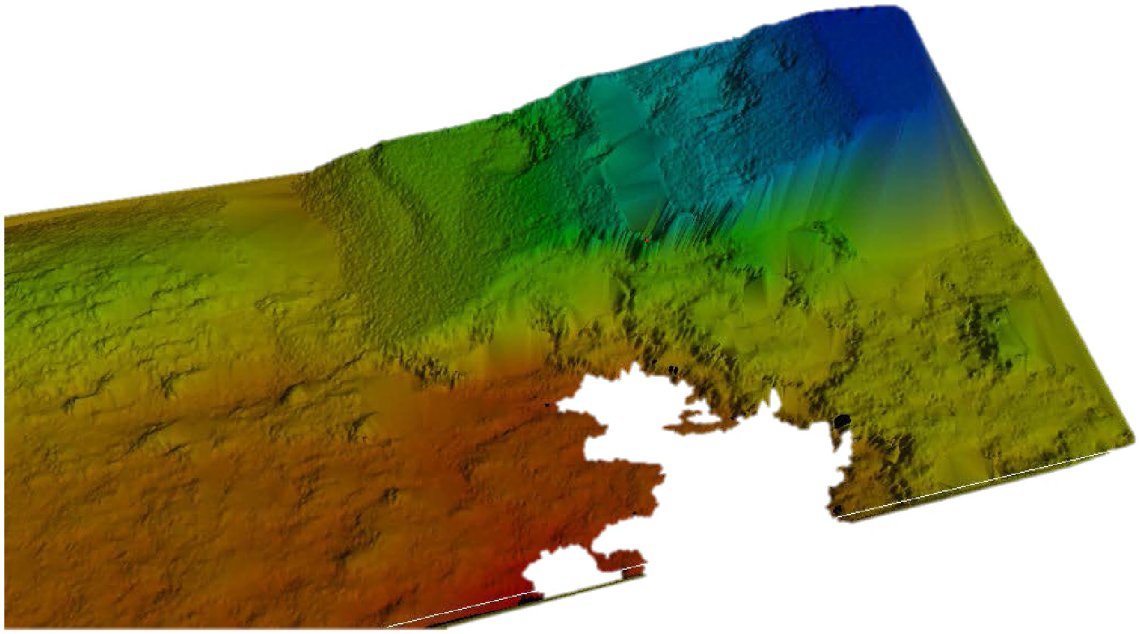

Figure 43 Scour hole of breach

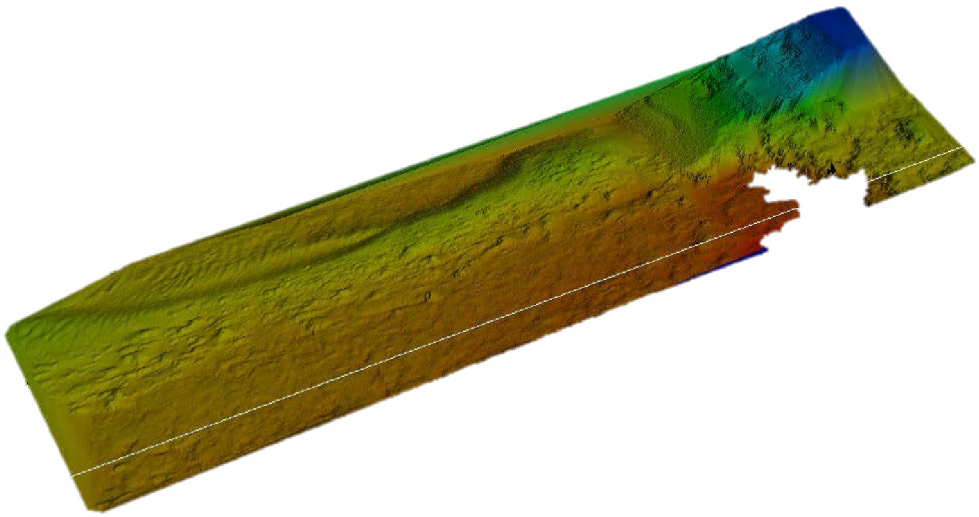

Figure 44 Topography of the whole flume model

Figure 45 Model Overview from the Downstream

The breach channel (Fig. 46) was 2.5 m wide and the side breach slope was very steep with negative value at some location due to the undermining process of helicoidal erosion. The material of the front embankment was eroded by the upstream convergent flow. The upstream breach width is larger than the downstream ones, e.g., 0.21m in Model 4.

Figure 46 Model Overview from the Upstream

7 Conclusions and Recommendations

In this project, 5 runs of breach experiment were conducted in a relative large flume. The experiments gave a strong support to the hypothesis that the cohesive embankment breach is a hydrodynamic process coupled with soil mechanics. The breaching starts with the initial erosion of the embankment surface and washes away the embankment surface. Due to the surface erosion at the toe of embankment, the headcut erosion is stimulated on the embankment slope. The headcut erosion can also develop into cascade headcut migration due to the non-homogenous characteristics of the embankment material. While headcut migration stimulates the breach to develop in longitudinal direction, the helicoidal erosion triggers the breach to widen in lateral direction. Three types of erosions (surface erosion, headcut erosion and helicoidal erosion) contribute to the erosion process of the breaching in embankment, however, the breaching flow is the driving force for the erosion. Sediment deposition in the breaching process is also of importance, generally ignored in the embankment breaching studies.

References

Dodge, R.A., 1988. Overtopping flow on low embankment dams − summary report of model tests. REC-ERC-88-3, U.S. Bureau of Reclamation, Denver, USA.

Fread D.L., 1988. BREACH: an erosion model for earthen dam failures. National Weather Service (NWS) Report, NOAA, Silver Spring, Maryland, USA.

Ralston, D.C., 1987. Mechanics of embankment erosion during overflow. Proceedings of the 1987 ASCE National Conference on Hydraulic Engineering, Williamsburg, USA, 733–738.

Visser P.J., 1998. Breach growth in sand-dikes. PhD thesis, Delft University of Technology, Delft, the Netherlands.

Zhao G., Visser P.J., Peeters, P., Vrijling J.K., 2013. Headcut Migration Prediction of the Cohesive Embankment Breach. Engineering Geology, Volume164, 2013, Pages 18-25.

Zhu Y.H., 2006. Breach growth in clay-dikes. PhD thesis, Delft University of Technology, Delft, the Netherlands.

Zhu Y.H., Visser P.J., Vrijling J.K., 2004. Review on embankment dam breach modeling, New Developments in Dam Engineering, Taylor & Gracis Group, London, UK.

Appendix list

B.1. Velocity Database

B.1.1. Velocity database for Run 1 (1 ADV , 3 electromagnetic velocity meters)

B.1.2. Velocity database for Run 2 (1 ADV , 3 electromagnetic velocity meters)

B.1.3. Velocity database for Run 3 (1 ADV , 3 electromagnetic velocity meters)

B.1.4. Velocity database for Run 4 (1 ADV , 3 electromagnetic velocity meters)

B.1.5. Velocity database for Run 2 (1 ADV , 3 electromagnetic velocity meters)

B.2. Water Level Database

B.2.1. Water level database for Run 1 (9 water level meters)

B.2.2. Water level for Run 2 (9 water level meters)

B.2.3. Water level for Run 3 (9 water level meters)

B.2.4. Water level for Run 4 (9 water level meters)

B.2.5. Water level for Run 2 (9 water level meters)

B.3. Topography Database

B.3.1 3DTopography per 5 minutes for Run 1 (3D Scanner)

B.3.2. 3DTopography per 5 minutes for Run 2 (3D Scanner)

B.3.3. 3DTopography per 5 minutes for Run 3 (3D Scanner)

B.3.4. 3DTopography per 5 minutes for Run 4 (3D Scanner)

B.3.5. 3DTopography per 5 minutes for Run 5 (3D Scanner)

B.4. Film Footage and Photo Database

B.4.1. Film Footage and Photo for Run 1 (2 high-speed video cameras above the flume and 3 high-speed video cameras side to flume, Photos)

B.4.2. Film Footage and Photo for Run 1 (2 high-speed video cameras above the flume and 3 high-speed video cameras side to flume, Photos)

B.4.3. Film Footage and Photo for Run 1 (2 high-speed video cameras above the flume and 3 high-speed video cameras side to flume, Photos)

B.4.4. Film Footage and Photo for Run 1 (2 high-speed video cameras above the flume and 3 high-speed video cameras side to flume, Photos)

B.4.5. Film Footage and Photo for Run 1 (2 high-speed video cameras above the flume and 3 high-speed video cameras side to flume, Photos)

B.5. Soil Mechanics Test Result Database

B.5.1. Soil test for Model 1

B.5.2. Soil test for Model 2

B.5.3. Soil test for Model 3

B.5.4. Soil test for Model 4

B.5.5. Soil test for Model 5